

Failure analysis of surface-micromachined microengines

Kenneth A. Peterson, Paiboon Tangyunyong, and Alejandro A. Pimentel

Electronic Quality/Reliability Center, Sandia National Laboratories, M/S 1081

P.O. Box 5800, Albuquerque, NM 87185-1081, USA

ABSTRACT

Microelectronic failure analysis (FA) has been an integral part of the development of state-of-the-art integrated circuits. FA of MicroElectroMechanical Systems (MEMS) is moving from its infancy to assume an important role in the successful design, fabrication, performance and reliability analysis for this new technology. In previous work¹, we focused on the application of several techniques developed for integrated circuit analysis to an earlier version of a surface micromachined microengine fabricated at Sandia. Recently, we have identified important new failure modes in binary counters that incorporate a newer design of the microengine, using a subset of integrated circuit failure analysis techniques including optical microscopy, focused ion beam (FIB) techniques, atomic force microscopy (AFM), and scanning electron microscopy (SEM). The primary failure mode we have identified is directly related to visible wear on bearing surfaces. In this paper, we describe in detail the characteristics of the failure modes in binary counters. We also compare the failure characteristics with those of an earlier version of the microengine.

Keywords: MEMS, Microengine, Failure Analysis, Wear Debris, Focused Ion Beam, Voltage Contrast, Scanning Electron Microscope.

1. INTRODUCTION

As MEMS technology has grown, a range of analytical techniques has been used to provide feedback that is necessary for design modifications, production process changes and failure analysis (FA) on prototype units involved in life testing. Several FA techniques that were developed and refined for FA of integrated circuits have been successfully applied to analyze MEMS. The small scale of MEMS devices has made an extension of several of these techniques very natural. This work emphasizes the application of these FA techniques to analyze microengines developed and fabricated at Sandia². Several designs of microengines have been studied in detail to identify their failure modes. Our previous work¹ focused primarily on the early design of the microengines.

This work focuses on the study of new version of the microengines that has been incorporated into a binary counter. The results from the early microengines are also included in this work for comparison. The early and new versions of microengines are shown in Fig. 1a and Fig. 1b respectively.

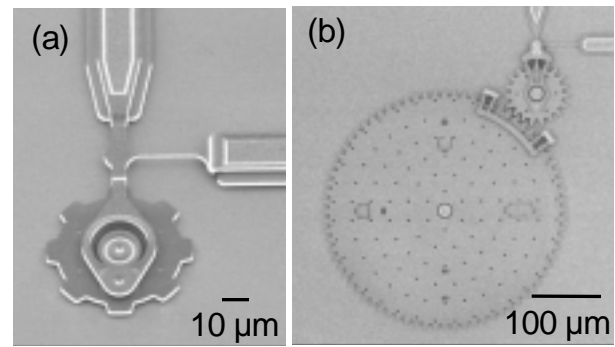


Figure 1. (a) An early design of microengine. (b) A binary counter, incorporating a new version of microengine that includes several modifications in both design and processing.

The microengines described in this paper were fabricated on silicon wafers using Sandia's Ultra-planar Multi-level MEMS Technology (SUMMiT). SUMMiT involves similar fabrication processes (deposition, patterning and etching) to those used in integrated circuits. SUMMiT also incorporates multiple polysilicon layers which are freed simultaneously from encapsulating glass in the release etch. Chemical-Mechanical Polishing (CMP) is also used in the fabrication process.

All of the microengines (both early and new designs) are actuated by two orthogonal sets of electrostatic comb drives (Fig. 2), with each axis having bi-directional drive capability. These comb drives consist of comb fingers attached to "wings" that are attached to a shuttle which can be thought of as the backbone of the comb drive. Springs serve to suspend the shuttle above a ground plane, to provide an electrical ground potential to the shuttle, and to restore the engine at rest to its equilibrium position. The driving ends of the shuttle are connected to the link arms. The link arms are, in turn, coupled to each other and then to the drive gear through a pin joint (Fig. 3). The

areas underneath the combs and the gears are electrically grounded planes. The drive gear is actuated by providing appropriate electrical signals to the comb drives^{3,4}. Typically, half sine waves of variable amplitudes and frequencies in 90-degree phase step are applied to the appropriate fixed combs of the electrostatic comb drives. Recently, a new software developed for reliability studies has been added to provide diagnostic signals. The motion of the drive gear is constrained by the flanged hub (Fig. 3) on which the gear rotates, as well as by all the linkages connecting the comb drives to the gear. In the binary counter, an additional large load gear is coupled to the drive gear. Besides the additional load gear, there are other modifications in the design of the binary counter to accommodate the additional load from the load gear. The comb drives, for example, are “double deck” instead of “single deck” in the early version. The “double deck” design, in conjunction with changes in the dimensions of the comb drives, allows the combs to deliver more force to drive the load gear. The gear teeth in the binary counter are also much better for driving because they are fully involute unlike the crude teeth in the early version.

In this paper, a failure in the binary counter is defined as the inability of the microengine to make a complete revolution in the drive gear during the inspection period.

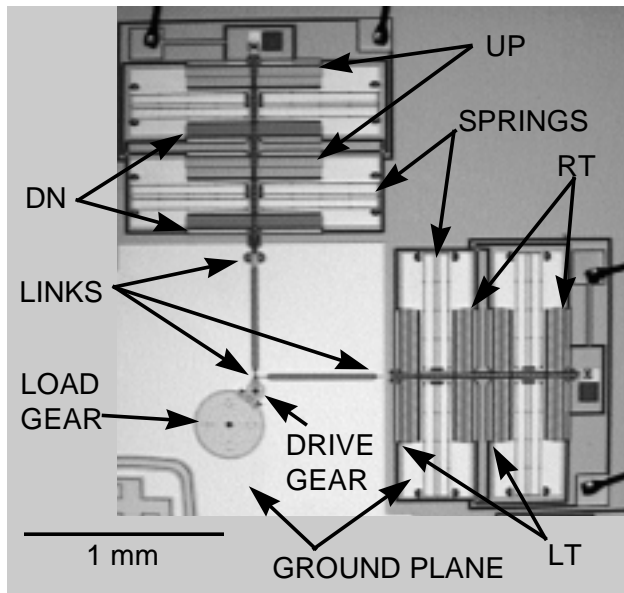


Figure 2. A low-magnification optical image of a binary counter (See arrows for various components including sets of combs to pull the shuttle to the right (RT), left (LT), up (UP), and down (DN) through link arms (links).

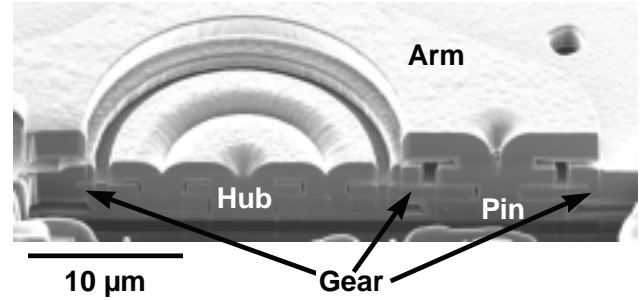


Figure 3. Focused ion beam (FIB) cross section of the drive gear and pin joint in a binary counter.

2. FAILURE ANALYSIS TECHNIQUES

2.1 Optical Microscopy

Optical microscopy is one of the most valuable and widely used tools in the FA of MEMS. In addition to permitting observations of the obvious, such as which elements are functioning properly and verification of the failures, it can provide a quick initial view of small defects. The features that can be observed optically include textures, stains, debris, fracture, and abnormal displacements. Figure 4, for example, shows evidence of wear debris in the gap between the gear and the hub. Optical inspection is also very useful, particularly at very high magnifications (for example using 50X or 100X objectives), for detecting minute displacements in non-functional or stuck microengines. These minute displacements can, for example, provide clues of where and why the movable components in the microengines are stuck. Videotaping

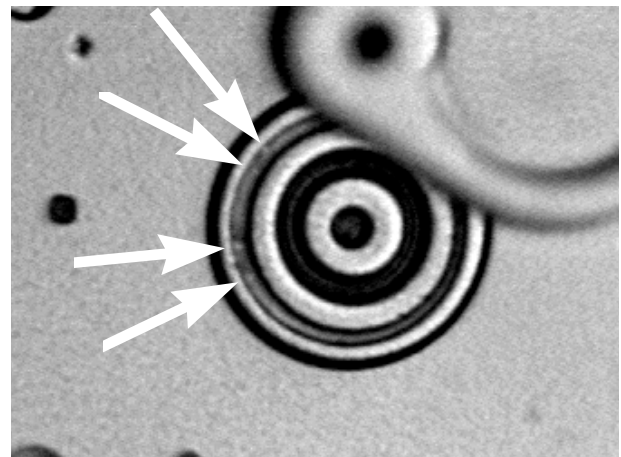


Figure 4. A high-magnification optical image showing wear debris in the gap between the drive hub and drive gear in a failed binary counter.

of the operating engines have also proven to be very useful for tracking performance during tests of operating lifetimes⁵.

2.2 Scanning Laser Microscopy (SLM)

Scanning laser microscopy has been used primarily to obtain confocal images. A confocal image is an image with a very limited depth of field (depth of focus) created by inserting an aperture in the optical path. By taking a series of confocal images at different focal planes, an extended depth-of-focus image can be constructed. The extended depth-of-focus image is particularly useful in resolving elements which have abnormal vertical displacements. Figure 5 shows an example where a malfunctioning comb drive was not free to translate in-plane, but did deform out-of-plane under power. The image in Figure 5 was obtained by subtracting an unpowered extended depth-of-focus image from the powered one. The grayscale in the image represents different sample heights. Bright area indicates a larger height. Figure 5 shows both the low-magnification and high magnification images of comb drives and the shuttle. The bright area shown in the shuttle and the movable comb areas indicates that these two components of the microengine levitate under power. The fixed combs do not change height under power and appear dark in the image.

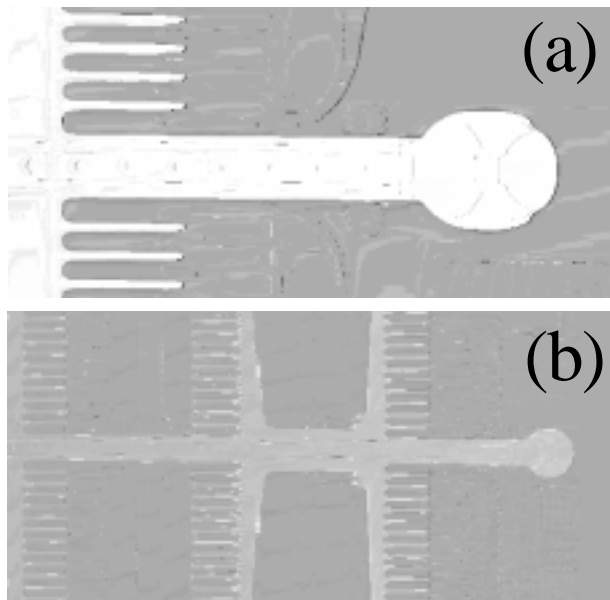


Figure 5. (a) A high-magnification and (b) a low-magnification extended depth-of-focus images of movable comb and shuttle in a binary counter showing levitation of both components under power.

2.3 Scanning Electron Microscopy (SEM)

The SEM has been useful for imaging defects at high magnification as well as determining electrical continuity in static and operating microengines. Figure 6 shows a conventional use of secondary electron imaging in the SEM to identify a broken spring element in the comb drive of a failed binary counter.

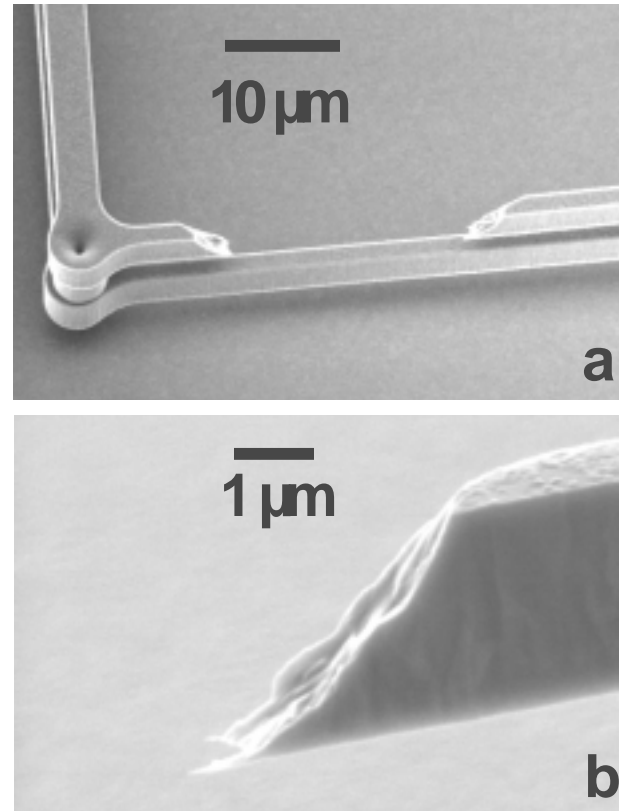


Figure 6. SEM images of broken upper decks on spring elements.

Secondary electron imaging in the SEM was also helpful in identifying the only wear track ever identified on an early version of the microengine, as shown in Figure 7. This wear track is likely to have resulted from an anomaly involving the particle shown at the left in Figure 7. The non-concentric track could only have been made by a gear/hub assembly which had a broken point of attachment to the substrate (shown at center). In another example, Figure 8 shows the wear debris on the intact drive gear. Figure 9 also shows the wear debris in the receiver hole for the drive gear of a failed binary counter after the pin has been fractured and the gear removed.

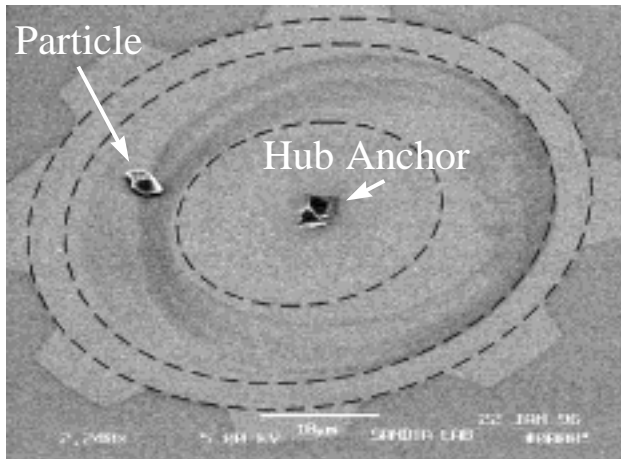


Figure 7. SEM image of a wear track related to a particle on the substrate. Concentric circles show the relationship of the track to the gear geometry. Note that the hub attachment is fractured (shown at center).

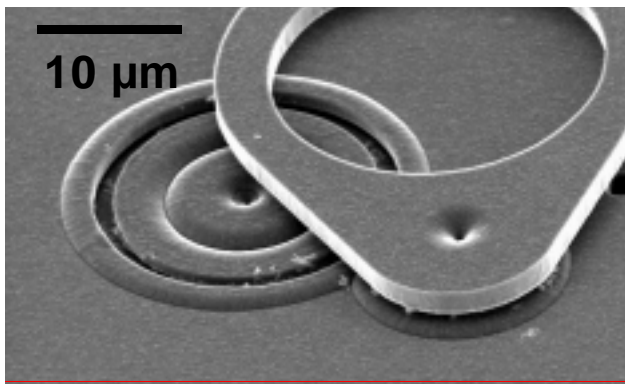


Figure 8. SEM image of a drive pin and a drive gear showing wear debris on the hub of the drive gear.

Passive and active voltage contrast techniques have identified structures at potentials different from those expected. Passive voltage contrast is defined as contrast which arises from voltage differences induced by rastering the beam causing various elements reach an equilibrium potential through self-charging. Active voltage contrast is defined as that arising from external application of voltage on different structures. In both cases, contrast is generated by differences in secondary electron emission yields caused by differences in surface potential. When imaging with a primary beam energy of 1keV, areas that are at positive potential appear dark in the images and those that are at ground appear bright. It has been possible, by increasing the accelerating potential, to observe a polarity change in the features which were charging, due to a crossover in the secondary electron emission efficiency. Figure 10 shows a passive voltage

contrast image of a gear and link arms with pin joints. The passive voltage contrast shows that the electrically floating arms and gear are charged positively (dark) with respect to the gear hub and shuttle, which have direct contact to ground. The passive voltage contrast image of Figure 11 shows a microengine with flexible links which provide a direct connection to ground through the shuttle and springs. In this case, the indirect contact is between the gear and link at a pin joint and between the gear and its hub. In the flexible link case, only the gear is charged positively with respect to the grounded elements.

Changes in voltage contrast were observed among several load gears in Figure 12. For example, the left load gear appears dark in Figure 12 (charged positively) compared to the other two. Voltage contrast differences were also observed between the load and the drive gear in each binary counter.

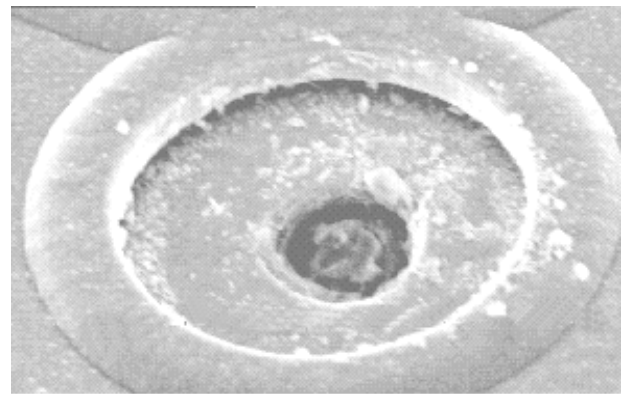


Figure 9. SEM image of wear debris in the receiver hole for the drive gear of a failed binary counter after the pin has been fractured.

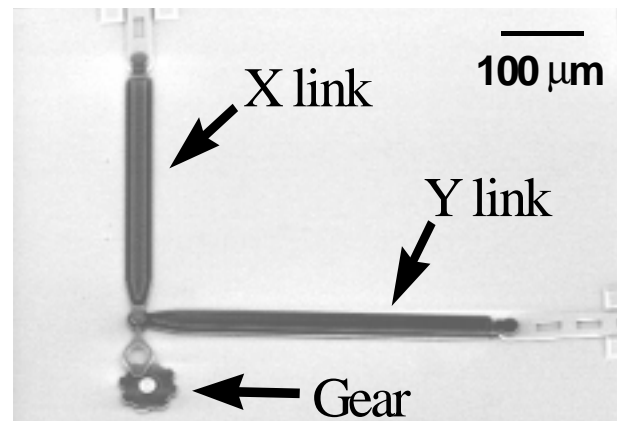


Figure 10. Passive voltage contrast showing charging of link arms and gear at 1 keV in the SEM.

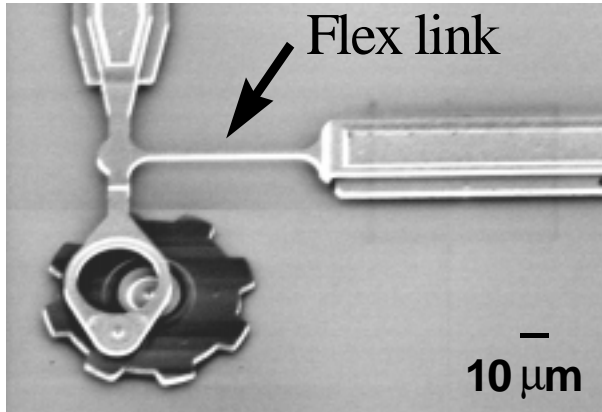


Figure 11. Passive voltage contrast showing charging of the gear only with respect to ground plane, hub, and link arms at 1 keV in the SEM. Arrow indicates flexible link.

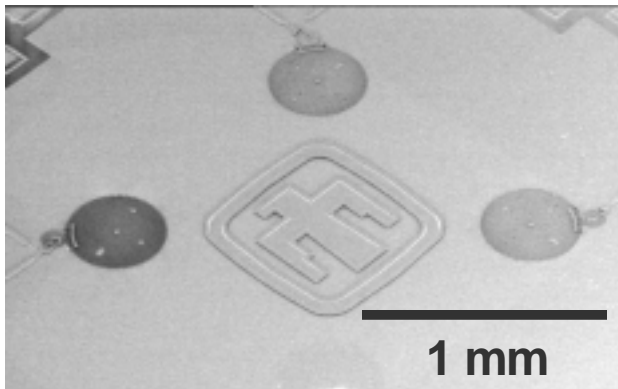


Figure 12. SEM image showing changes in voltage contrast among three load gears. Voltage contrast differences were also observed between the drive gears and load gears in the binary counters.

The same electrical feed-through capability which permits active voltage contrast imaging has been used to successfully operate microengines in the SEM in a high-vacuum environment. Some microengines stopped running during and following electron beam irradiation, while others were operated for hours even with continuous beam exposure. During the operation of one such engine, the electrically charged gear and pin-jointed links were seen to discharge once per revolution. The voltage contrast on the ground was also seen to change periodically per revolution. This change in voltage contrast behavior can be attributed to the intermittent contact between grounded and powered features in the microengine that occurs during the engine's operating cycle. The voltage contrast shift on ground planes has also been observed in the focused ion beam (FIB).

2.4 Focused Ion Beam (FIB)

The focused ion beam (FIB) uses a 30 keV beam of positive gallium ions (Ga^+) to irradiate the surface of the sample in a defined area. This irradiation causes surface charging, which can be neutralized by a flow of low energy (~ 30 eV) electrons from a flood gun. Images can be made using a signal consisting of either secondary ions or secondary electrons with or without charge neutralization by the electron flood gun. The FIB has been used to image structures, to cross section elements of concern (as seen in Figure 3) and to cut elements free for subsequent examination. One interesting result is the observation of motion of the structures during irradiation by the ion beam. Figure 13 shows a gear which, as submitted for FA, appeared to be stuck on the hub. The gear moved freely, however, after initial FIB examination using charge neutralization with the electron flood gun.

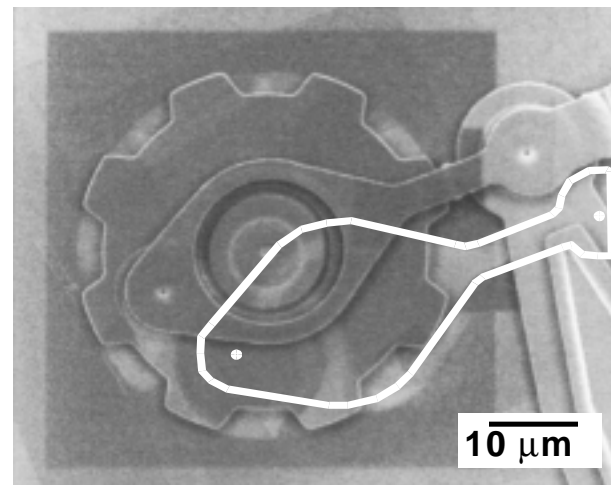


Figure 13. Evidence of charging effect from the ion beam on MEMS structures. The "stuck" position of the X link is outlined in white.

Another use of FIB milling is to gain access to bearing surfaces which are normally hidden from view. By careful microsectioning, gears and pins have been separated. Using fine probes at a probe station, it has been possible to mechanically nudge elements to orientations where they can be carefully examined in the SEM as shown in Figure 14. This figure shows one half of a separated gear that has been flipped over to examine the back surface and the other half remaining upright but separated from the hub. This operation required extreme care, as the slightest vibration, or the existence of static charge caused these small pieces to be ejected from the sample.

After separation, the bearing surfaces of the gears were carefully examined in the SEM. Figures 15 and 16 show

the front and back bearing surfaces of a gear which was operated until failure due to non-uniform rotation. These show a typical result which is the lack of physical indications of wear in the early microengine.

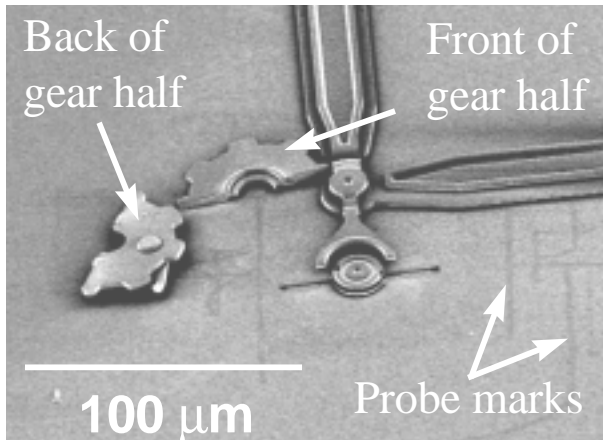


Figure 14. Microengine gear which has been micro-sectioned in the FIB and separated for SEM examination of bearing surfaces.

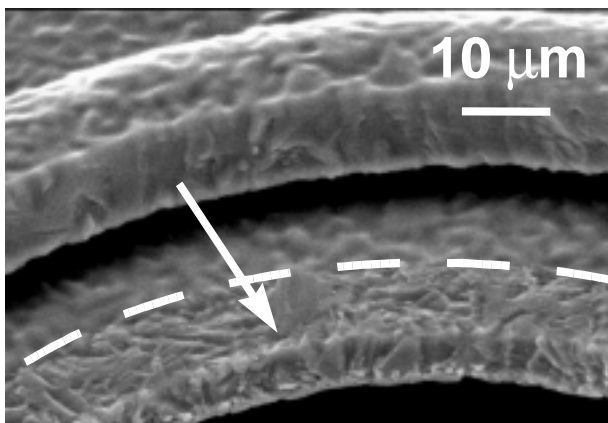


Figure 15. Top and inner surface of gear operated to failure. Arrow and dashed line indicate bearing surfaces.

Passive and active voltage contrast imaging using FIB without charge neutralization⁶ has also been useful on MEMS. For example, passive voltage contrast accounts for the dark appearance of the gear in the cross section of Figure 17, as it is electrically isolated in encapsulating glass and thus acquires a positive charge

One complication from using the FIB has been observed. Sputtered material can redeposit from the area being milled in a line of sight fashion on the undersides of suspended members. This can create the appearance of a separate layer, such as the light contrast layer visible in the FIB section of Figure 3. This material is thickest at

the milled edge, tapering back into the sample. Because this redeposited material is masked from the bearing surface by the flange of the hub, it might be confused with a wear track on the gear. An example of this is shown in Figure 18.

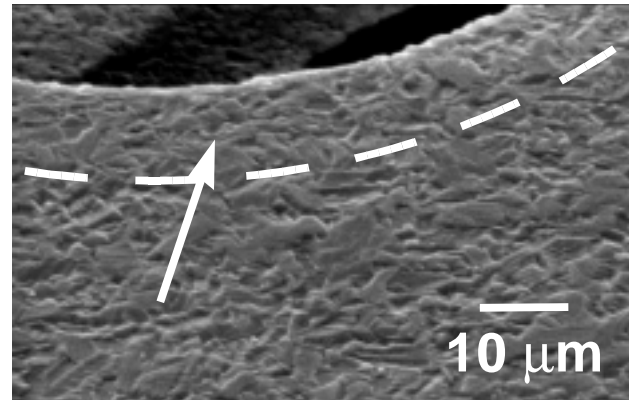


Figure 16. Back surface of gear operated to failure. Arrow and dashed line indicate bearing region.

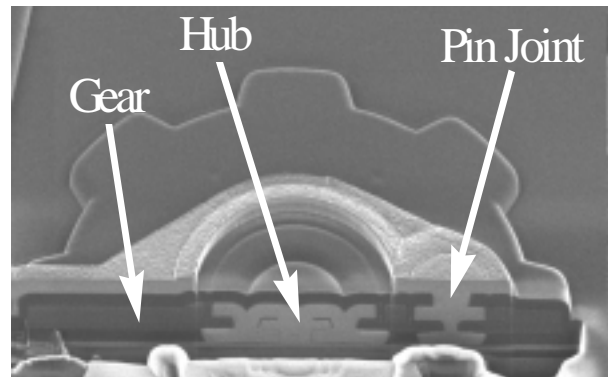


Figure 17. FIB section of unreleased gear showing different voltage contrasts between hub/pin joint and gear.

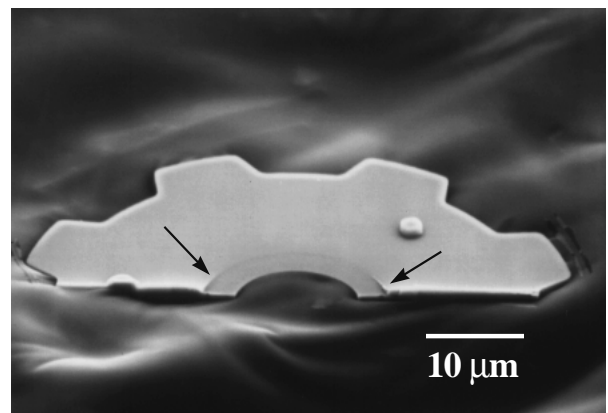


Figure 18. Micro-sectioned gear bottom surface showing FIB re-deposited material (arrows).

2.5 Atomic force microscopy (AFM)

The atomic force microscope (AFM) provides very detailed topographic images and surface traces. Figure 19 shows the wear debris on the drive gear of a failed binary counter similar to those shown Figures 8 and 9. AFM was also used to measure the surface roughness of the wear track shown in Figure 7. Figure 20 shows a topology image of an area which includes the wear track. Smoothing was observed in the track, compared to the region outside the track. A line scan across the track is shown in Figure 21.

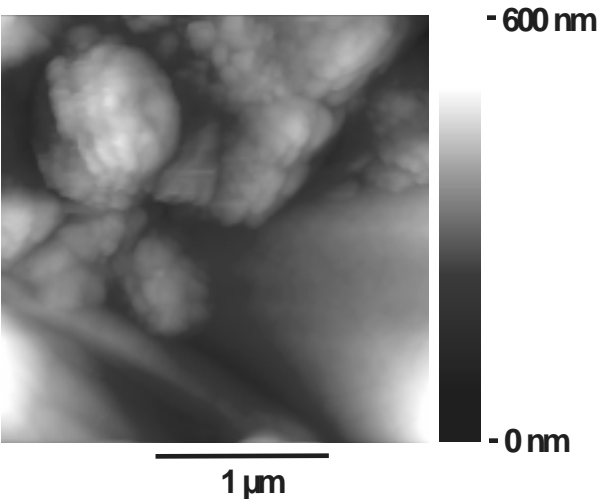


Figure 19. AFM image of wear debris on a drive gear of a failed binary counter.

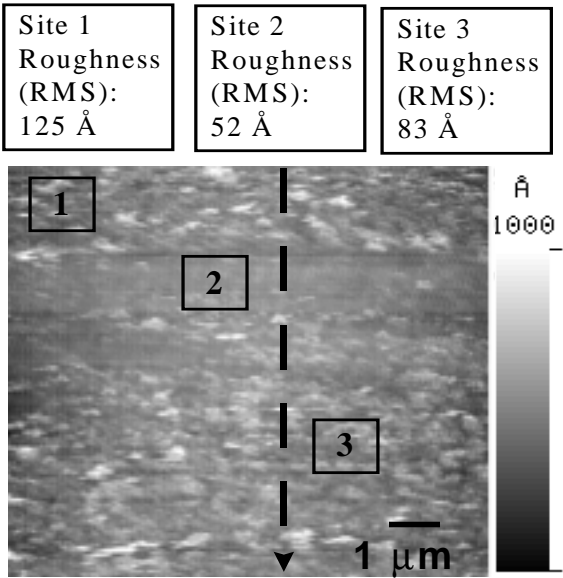


Figure 20. AFM topology image of wear track. The dashed line indicates the position of line scan of Fig. 23.

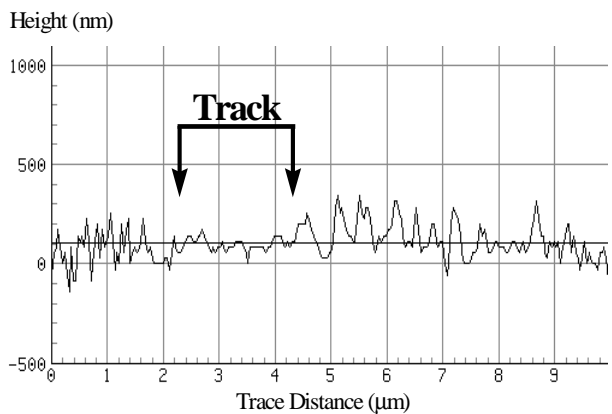


Figure 21. Topology line scan across wear track in Figure 20.

2.6 Infrared Microscopy

Several operating microengines were examined using an infrared microscope to construct thermal images based on the infrared radiance emitted from the structures. Figure 22 shows thermal image of the X-comb drives of an early version of microengines which was operating, but rotating irregularly with a pause in the rotation cycle. Hot spots (areas where the radiance increased in the image) were found in the X-comb drives. In gray scale, the hot spots appear dark, and are indicated by arrows in Figure 22. No hot spots were found in the Y- comb drives, nor were found in the comb drives of engines operating with smooth rotation.

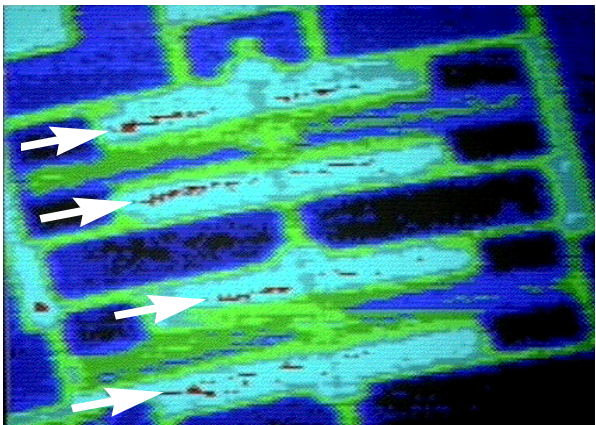


Figure 22. Infrared image of defective operation in early version of microengine showing hot spots (dark in appearance) in X-comb drive area.

2.7 Light Emission

The possibility of arcing at combs suggested the use of light emission analysis, which is common in FA of ICs. The same microengine which exhibited the hot spots in Figure 22 was analyzed using light emission, but no

emitted light was detected under the same operating conditions.

2.8 Acoustic Microscopy

Acoustic microscopy was employed on stationary microengines in an attempt to resolve contact between stuck gears and links and the substrate. This technique is more destructive to the sample due to the introduction of water as a coupling fluid. The acoustic signal could not be translated into evidence of sticking, although morphological features were resolved.

2.9 Acoustic Emission

Acoustic emission was also evaluated on several engines while they were running. This involved the attachment of a sensor to the package containing the microengines and “listening” for acoustic events as microengines were operated. No signal was resolvable above the background noise level

2.10 Laser Cutting

A laboratory laser cutter has been used to excise portions of circuits and sever connections to determine which elements are free or stuck. It has also been used to impart energy to members such as gears and links which moves like a shock wave to agitate discrete portions of the overall system.

2.11 Lift-off Technique

Careful removing elements of a microengine with a conductive laboratory adhesive tape used for SEM mounting has added another dimension to the analysis of microengines. The lift-off technique allows examination of the bottom surfaces of engines (Fig. 23) that provide additional information (such as the accumulation of wear debris or evidence of damage to pin receiver holes) for determining failure modes of the defective and failed microengines.

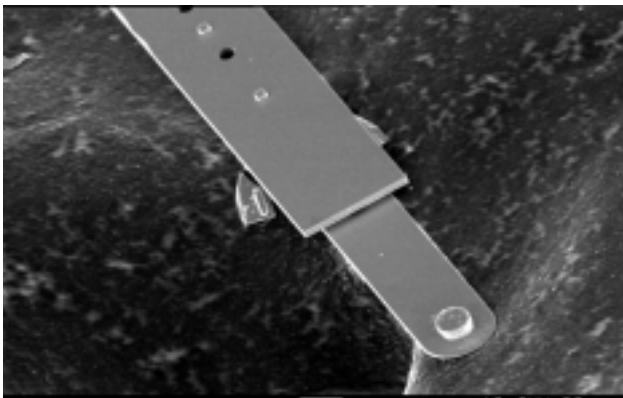


Figure 23. SEM image of a pin-joint shuttle which was lifted off using conductive adhesive tape.

3. RESULTS AND DISCUSSION

3.1 Early Version of Microengine

There were two types of failure modes that were observed in the early microengines: obvious and non-obvious. The obvious failure modes are normally catastrophic and the root causes can be easily identified with failure analysis techniques described in previous section. Failure modes such as lateral and vertical comb finger sticking, and fracture of components (e.g., spring fracture) are in this category. Non-obvious failure modes are non-catastrophic and more elusive. The root causes of this type of failures cannot be easily identified by application of standard FA techniques. Existence of intermittence in microengines, either as fabricated, or as a result of brief or extended operation belongs to this category. The degradation or failures of microengines can be attributed to a variety of causes⁷. Examples of the root causes are described below.

3.1.1 External Particulate Contamination

External particulate contamination outside the clean room environment, where reliability testing and failure analysis is conducted, is minimized by the use of transparent covers taped to ceramic packages. Particles could naturally be expected to have a detrimental mechanical or electrical effect on devices where small gaps exist between bearing surfaces or elements with large potential differences. Particulate contamination has been a minor problem and has not received the main attention for this study. The particles which receive attention are those which might be internally generated, or present in spite of a clean room environment. An example of a particle was shown in Figure 7.

3.1.2 Fused Components due to Overdriving

A condition that results from overdriving leading to inadvertent contact of structural and electrical members has been observed in springs and in comb fingers. Overdriving occurs when large voltages were applied to the comb drives. The relatively high voltages employed make arcing possible in these cases, and attachments resembling a weld can result. These attachments are occasionally small enough to be subsequently freed without extensive damage, but more often are permanent.

3.1.3 Sticking

Sticking can affect even elements that are not powered. Sticking can be attributed to the presence of capillary force between two surfaces. Sticking due to capillary force can be reduced with the application of drying techniques such as freeze sublimation or super-critical

drying. Sticking can also be mitigated by coating potential contacting surfaces with hydrophobic chemicals.

3.1.4 Electrostatic Clamping of Gears (Links)

Electrostatic charging of MEMS elements, such as electrically isolated gears and links, has been noticed in both the SEM and the FIB. Charging of comb drives has also been induced from laser pulses in their vicinity. Electrostatic attraction has also been evident on MEMS elements as they were manipulated with probe tips for the purpose of SEM imaging. Pieces frequently clung to the tips of the probes and were difficult to free.

There are three pieces of evidence that suggest the possible existence of electrostatic clamping at the gear. The first piece of evidence was obtained by observing the behavior of a stuck gear while it was irradiated in the FIB. The number of scans of the gear and links were limited to a few, since the beam is continuously removing material from the surface. The field of view, approximately 100 μm , was slightly larger than the gear diameter. After the area was subjected to several scans with charge neutralization enabled, the gear suddenly sprung to its rest position. This phenomenon was observed several times, and occurred only while the charge neutralization was enabled.

The second piece of evidence was observed during SEM illumination of operating microengines. Engines operating normally at 1 keV beam were temporarily clamped when the electron beam energy was increased to 5 keV. These clamped engines then resumed normal operation when the beam energy was again reduced to 1 keV. The clamping and unclamping of the microengines can be attributed to the fact that the microengines are charged up differently at 1 keV and at 5 keV. At 1 keV, the engines are charged up negatively while they are charged up positively at 5 keV.

The third piece of evidence of clamping was observed during FIB irradiation of operating microengines. Illuminating only the gear and a portion of the links, with charge neutralization off, caused several flex-joint engines to operate for several revolutions and then become clamped. The clamped gears almost always started to rotate after charge neutralization was applied. The electrostatic clamping behavior was also found to be very sensitive to the scan size. The electron flood gun current density is constant for a given FIB current, whereas the ionic current density increases with smaller scan size. At smaller scan sizes and with charge neutralization enabled, the charging of the positive ion beam overwhelmed the neutralizing effect of the electron beam and, as a result, an operating engine became clamped. Increasing the scan size reduced the charging effect and the clamped gear started to rotate. These clamping and unclamping as a

function of scan sizes was very repeatable for several microengines.

3.2 Binary Counter

The majority of failures such as lateral and vertical comb finger sticking, and failure due to overdriving have been significantly reduced by changes implemented in both design and processing in the binary counter. Fracture of components such as fractured springs were also observed in the binary counter, but this type of failure was mainly due to the improper handling. In contrast to the early microengines where no evidence of wear was observed, the primary failure mode in the binary counter is wear. Wear debris is most common at drive pins (Figure 9) and at drive hubs (Figure 24). Wear debris has also been observed at the up-down shuttle and guide (Figure 25). Severe drive pin wear and occasional breakage of drive pins was the main characteristic of the binary counter when tested to failure. Figure 26, for example, shows the FIB cross sections of the drive gears for two samples with identical processing history. The upper image in Fig. 26 is a control device that was not tested and did not show any sign of wear. The lower image is a device that was tested to failure. Clearly, the tested part shows severe wear at bearing surfaces and surrounding areas. The most severe damage occurs at the pin where its diameter is significantly reduced. Even though there was severe wear in the drive gear, no evidence of wear was observed in the load gears for all the binary counters that were tested to failure. Auger electron spectroscopy of the wear debris indicated that silicon present in the debris was oxidized.

The presence of wear in binary counters and its absence in the early microengines can be attributed to the large stress experienced by the drive gear of the binary counter during the engine operation. In the binary counter, the magnitude of force required to operate the engine is at least several times larger than that in the early microengine. The larger force results in larger stress at the bearing surface on the drive gear particularly at the pin joint where severe wear was observed. The stress on the load gear, on the other hand, is relatively low and no evidence of wear was observed.

In addition to wear, other failure modes such as friction welding have also been observed in the binary counter. Figure 27, for example, shows the SEM image of the up-down shuttle of a failed binary counter. From visual and SEM inspection, the dimple of the adjacent guide appeared to be stuck to the shuttle. A FIB cut (the location of FIB cut is shown in Figure 27) was then performed to sever the connection between the portion of the guide supporting the dimple and the shuttle. After the FIB cut (Figure 28), the shuttle was able to move and drive the gears to rotate (Figure 29).

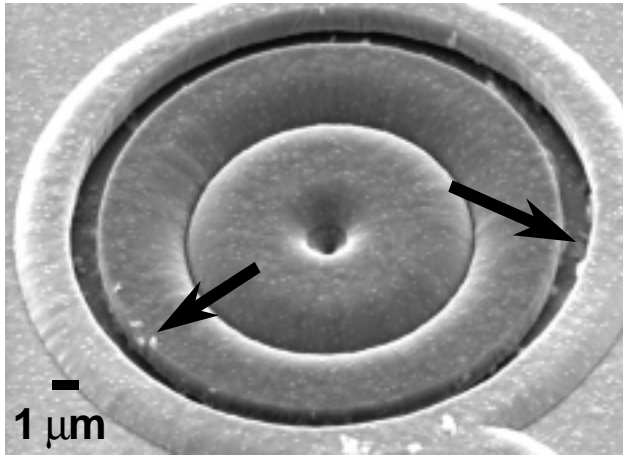


Figure 24. SEM image of characteristic wear debris on drive gear and hub in a failed binary counter.

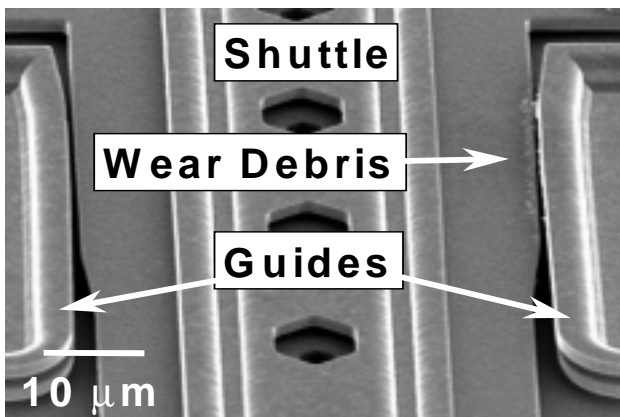


Figure 25. SEM image of wear debris on the shuttle and guide

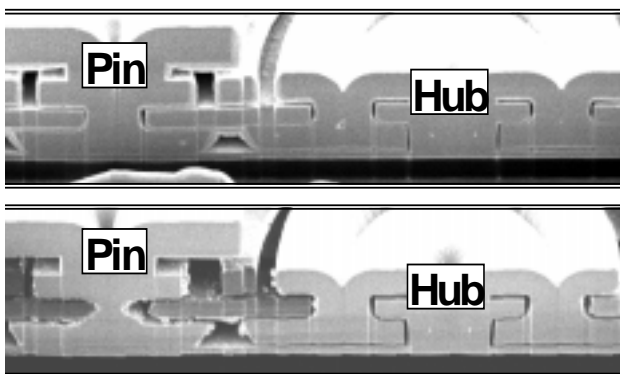


Figure 26. FIB cross sections of the drive gear of a binary counter that was not tested (upper) and one that was tested to failure (bottom). Note that no wear debris was observed in the upper image and severe wear was observed in the lower image.

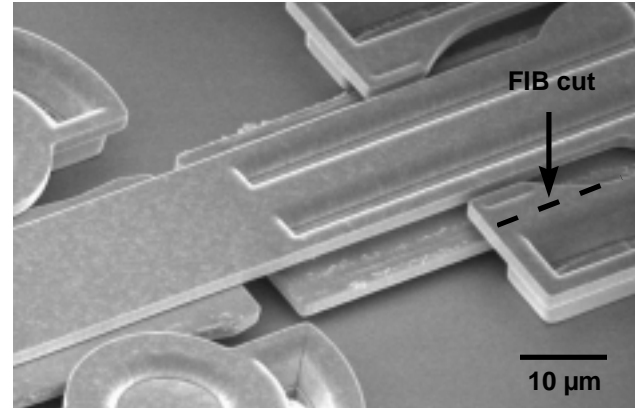


Figure 27. Location of FIB cut on the pinned link microengine guide of the up-down shuttle in a failed binary counter.

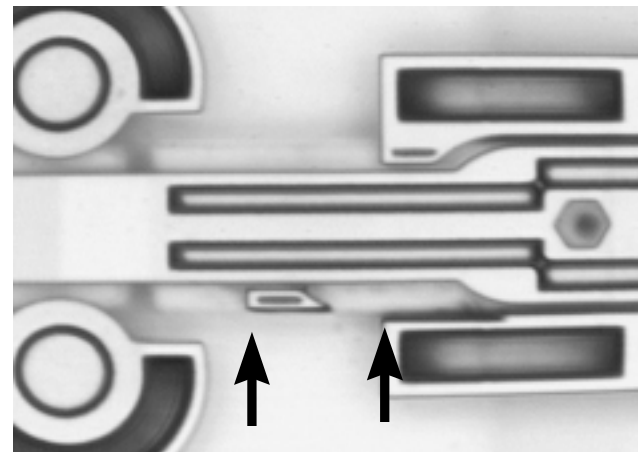


Figure 28. Optical image showing portion of the guide was severed by FIB cut and moved to the left. The FIB cut freed the shuttle from the guide.

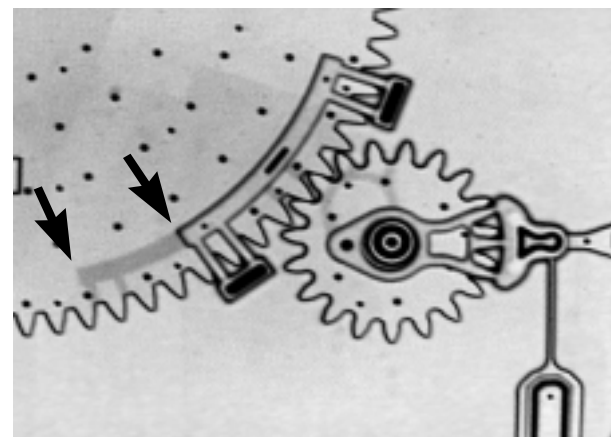


Figure 29. Rotation of load gear shown by arrows and associated FIB stains from initial position of system after portion of the guide was severed.

Intermittence was also observed in the binary counter. Similar to the early microengine, the root causes of the intermittence cannot be easily identified. Intermittence remains the most elusive type of failure in both the early microengines and the binary counter.

4. CONCLUSIONS

Several of the FA techniques that are commonly used in FA of integrated circuits have been very successful in analyzing and identifying failures in MEMS. The majority of failures observed in the early microengines such as lateral and vertical comb finger sticking, fractures of components and failure due to overdriving have been significantly reduced by changes implemented in both design and processing in the binary counter. The most dominant failure mode in the binary counter is wear. Wear debris is most common at drive pins in the drive gear where the stress is maximum. Other failure modes such as friction welding were also observed in the binary counter. The most elusive failure mode in binary counter continues to be intermittence with no visible physical characteristics, as experienced in early microengines.

5. ACKNOWLEDGEMENTS

The authors would like to thank John Gieske for acoustic microscopy, Alan Beattie for help with acoustic emission analysis, and Wayne Buttry for Auger Electron Spectroscopy analysis. Sandia is a multiprogram laboratory operated by Sandia Corporation, a Lockheed Martin Company, for the United States Department of Energy under Contract DE-AC04-94AL85000.

6. REFERENCES

1. K. A. Peterson, P. Tangyonyong and D. L. Barton, "Failure Analysis for Micro-Electrical-Mechanical Systems (MEMS)," Proceeding of the 23rd International Symposium for Testing and Failure Analysis, Santa Clara, October 27-31, 1997, pp. 133 – 142.
2. E. J. Garcia and J.J. Sniegowski, "Surface micromachined microengine," *Sensors and Actuators A* 48 (1995) 203-214.
3. S. L. Miller, J. J. Sniegowski, G. LaVigne, and P. J. McWhorter, "Performance tradeoffs for a surface micromachined microengine," *Proc. SPIE Micromachined Devices and Components II*, Vol. 2882, Austin, October 14-15, pp. 182-191, 1996.
4. S. L. Miller, J. J. Sniegowski, G. LaVigne, and P. J. McWhorter, "Friction in surface micromachined microengines," *Proc. SPIE Smart Electronics and MEMS*, Vol. 2722, San Diego, Feb. 28-29, 1996, pp. 197-204.
5. D. M. Tanner, N. M. Smith, D. J. Bowman, W. P. Eaton, and K. A. Peterson, 'First reliability test of a surface micromachined microengine using SHiMMeR,' *Proc. SPIE Micromachined Devices and Components*, Vol. 3224, Austin, September 29-30, 1997, pp 14 - 23.
6. A.N. Campbell, J. M. Soden, R. G. Lee, and J. L. Rife, "Electrical biasing and voltage contrast imaging in a focused ion beam system," *Proc. Of the 21st Inter. Symp. For Testing and Failure Analysis*, Nov. 6-10, 1995, pp. 33-41.
7. S. L. Miller, G. LaVigne, M.S. Rodgers, J.J. Sniegowski, J.P. Waters, and P.J. McWhorter, "Routes to failure in rotating MEMS devices experiencing sliding friction," *Proc. SPIE Micromachined Devices and Components*, Vol. 3224, Austin, September 29-30, 1997, pp. 24 – 30.